AGU PUBLICATIONS

JGR

Journal of Geophysical Research: Space Physics

RESEARCH ARTICLE

10.1002/2014JA020333

Key Points:
- We develop a forecast models of solar proton flux profiles for well-connected SPEs
- We use a modified Weibull curve function to approximate a SPE flux profile
- We find that CME acceleration is an important factor for predicting proton flux profiles

Correspondence to:
Y.-J. Moon,
moonyj@khu.ac.kr

Citation:
Ji, E.-Y., Y.-J. Moon, and J. Park (2014), Forecast of solar proton flux profiles for well-connected events, *J. Geophys. Res. Space Physics*, *119*, 9383–9394, doi:10.1002/2014JA020333.

Received 25 JUN 2014
Accepted 21 NOV 2014
Accepted article online 27 NOV 2014
Published online 16 DEC 2014

Forecast of solar proton flux profiles for well-connected events

Eun-Young Ji[1], Yong-Jae Moon[2], and Jinhye Park[3]

[1]Division of Polar Climate Change, Korea Polar Research Institute, Incheon, Korea, [2]School of Space Research, Kyung Hee University, Yongin, Korea, [3]Department of Astronomy and Space Science, Kyung Hee University, Yongin, Korea

Abstract We have developed a forecast model of solar proton flux profiles (> 10 MeV channel) for well-connected events. Among 136 solar proton events (SPEs) from 1986 to 2006, we select 49 well-connected ones that are all associated with single X-ray flares stronger than M1 class and start to increase within 4 h after their X-ray peak times. These events show rapid increments in proton flux. By comparing several empirical functions, we select a modified Weibull curve function to approximate a SPE flux profile. The parameters (peak flux, rise time, and decay time) of this function are determined by the relationship between X-ray flare parameters (peak flux, impulsive time, and emission measure) and SPE parameters. For 49 well-connected SPEs, the linear correlation coefficient between the predicted and the observed proton peak fluxes is 0.65 with the RMS error of 0.55 $\log_{10}$(pfu). In addition, we determine another forecast model based on flare and coronal mass ejection (CME) parameters using 22 SPEs. The used CME parameters are linear speed and angular width. As a result, we find that the linear correlation coefficient between the predicted and the observed proton peak fluxes is 0.83 with the RMS error of 0.35 $\log_{10}$(pfu). From the relationship between error of model and CME acceleration, we find that CME acceleration is an important factor for predicting proton flux profiles.

1. Introduction

It is well known that solar proton events (SPEs) are mostly associated with strong flares and fast halo coronal mass ejections (CMEs) [*Reames*, 1999, 2013]. NOAA Space Weather Prediction Center (SWPC) defines the SPEs which have a flux of 10 particles cm^{-2} s^{-1} sr^{-1} in the > 10 MeV energy channel. The SPEs can affect commercial airlines in polar routes, electronic system on satellite, HF communication in ionosphere, extravehicular activity from space station, and manned space flight missions [*Feynman and Gabriel*, 2000]. Because of these damages, the forecast of SPEs has been regarded to be very important for space weather.

Several researchers have attempted to make SPE forecast models using associated solar phenomena [e.g., *Balch*, 2008]. The SPE forecast models can be classified as follows: (1) forecast of SPE occurrence probability from historical SPE data depending on flare or CME parameters [e.g., *Balch*, 1999; *Park et al.*, 2010, 2012], (2) forecast of SPE occurrence probability based on the logistic regression model and its magnitude [e.g., *Garcia*, 2004a; *Laurenza et al.*, 2009], (3) forecast of SPE peak fluxes [e.g., *Xapsos et al.*, 1998; *Balch*, 1999, 2008; *Kahler et al.*, 2007; *Garcia*, 2004a, 2004b], (4) forecast of the time between X-ray flare start or peak time and proton peak time [e.g., *Smart and Shea*, 1989; *Balch*, 2008], and (5) forecast of SPE flux profile [e.g., *Aran et al.*, 2005; *Luhmann et al.*, 2007, 2010; *Verkhoglyadova et al.*, 2009, 2010; *Núñez*, 2011]. Several models are now routinely in operation for real-time SPE forecast at the Web sites (e.g., http://www.swpc.noaa.gov/wmo/protons.php and http://spaceweather.uma.es/forecastpanel.htm).

It is still difficult to forecast SPE flux profiles because it is necessary to sufficiently understand the physical mechanisms of particle acceleration in the solar corona and transport of particles through the interplanetary space. There are several models for fitting proton flux profiles using numerical models [e.g., *Beeck et al.*, 1987; *Heras et al.*, 1992; *Lario et al.*, 1998]. These models, however, are fitting SPE flux profiles as a result of postanalysis. Several studies have been made for the forecast models of SPE flux profiles [*Aran et al.*, 2005; *Luhmann et al.*, 2007, 2010; *Verkhoglyadova et al.*, 2009, 2010; *Núñez*, 2011]. The models are able to forecast a SPE flux profile from its start to the arrival of its associated interplanetary shock at any point in interplanetary space [*Aran et al.*, 2005; *Luhmann et al.*, 2007, 2010; *Verkhoglyadova et al.*, 2009, 2010]. The model developed by *Aran et al.* [2005] is based on the numerical model of propagating coronal/interplanetary shock with SPE databases which contains the "synthetic" proton flux and fluence profiles upstream of the shock for 384 interplanetary scenarios. The model searches the profiles in the database for

those events with the closest characteristics to the input parameters. The model developed by *Luhmann et al.* [2007, 2010] predicts a SPE flux profile using a Center for Integrated Space weather Modeling MHD solar wind simulation model. This model includes a cone model of CMEs to initiate the related shock. They assume that the influence of shock evolution dominates over diffusive transport in determining the SPE time profiles. The SPE flux profile is simulated with a series of impulsive particle injections from the location of interplanetary coronal mass ejection shock on the sequence of observer-connected field lines. The model developed by *Verkhoglyadova et al.* [2009, 2010] predicts spectra and intensities of SPE using the Particle Acceleration and Transport in the Heliosphere (PATH) numerical code. The PATH code includes modeling a background solar wind, propagation of a CME-driven evolving shock throughout the inner heliosphere, particle injection into the moving shock, particle diffusion, and acceleration at the shock vicinity. Using the PATH code, they study the temporal evolution of the near-Earth energetic proton population in a SPE event and predict time-dependent spectra and intensity of SPE.

Our main interest is to forecast the flux profiles of SPEs in the > 10 MeV energy channel using flare and CME information. One similar study was carried out by *Núñez* [2011] who predicts the SPE flux profiles. They developed a dual model of empirical and regression for respectively forecasting the flux profiles of well-connected and poorly connected SPEs using soft X-ray and proton fluxes. The flux profile for model output presents "band" type which shows the uncertainty of SPE prediction. The model can forecast SPE flux profiles in real time, but it can only predict the profiles during their initial rise phases [*Núñez*, 2011].

The purpose of this study is to develop a forecast model of solar proton flux profile (> 10 MeV channel) from initial rise to decay phases for well-connected events. For this study, we select the well-connected SPEs among NOAA SPE events from 1986 to 2006. We find a best suitable empirical function to approximate a SPE flux profile. The paper is organized as follows. We briefly explain the data and the forecast model in section 2. We present the result and discussion of our study in section 3. A brief summary and conclusion are given in section 4.

2. Data and Method

2.1. Data

In this study, we use the soft X-ray data (1–8 Å) and proton data of > 10 MeV channel from GOES 5 to GOES 10. The X-ray and proton data are taken from the NOAA database (ftp://ftp.ngdc.noaa.gov/STP/space-weather/solar-data/solar-features/solar-flares/x-rays/goes/), and their time resolution is 5 min. We use 170 NOAA SPEs from 1986 to 2006. In the SPE list, we exclude 34 SPEs which do not have the location information of their associated flares.

Generally, the well-connected SPEs are defined as the events whose magnetic field lines are well connected to the site of shock acceleration, probably flare/CME source regions. They show rapid increments in solar proton flux, and most of the events occur in western region [*Reames*, 1999; *Cane and Lario*, 2006]. For this study, we quantitatively define the well-connected SPEs with the following conditions: (1) they are associated with X-ray flares stronger than M1 class (122/136), (2) their proton fluxes start to increase within 4 h after their associated X-ray flare peak times (60/122). There are two reasons why we decided 4 h after X-ray flare peak time. One is that the number of events is too small in case of 3 h. The other is that in case of 5 h, there are several events whose flux profiles are different from a typical one, (3) we exclude 11 SPEs associated with multiple flares and/or CMEs. Five events among 11 events are associated with the multiple CMEs studied by [*Ding et al.*, 2013, 2014; *Kahler and Vourlidas*, 2013, 2014]. Finally, we select 49 well-connected SPEs. We determine the start and end times of 49 events using observed proton flux data. The start times of SPEs are defined when there are noticeable enhancements in SPE flux for three consecutive data points after the corresponding X-ray flare peak times. The end times of SPEs are defined as the times when the proton fluxes just decrease to below 10 pfu after the proton peak times. The rise time is from start time to peak time of proton flux. The decay time is from peak time to end time of proton flux. Figure 1 shows a well-connected SPE with rise and decay times. As shown in Figure 1, the flux starts to increase just after the flare peak time and have a peak flux after 18 h. We examine the flux profiles of all 49 events and find that their typical patterns are quite similar to one another. Figure 2 shows a histogram of longitudes of 49 well-connected SPEs. We see that most of the events (46/49) are distributed in the western region. These 49 well-connected SPEs show the typical characteristics of events having rapid increment in the western region.

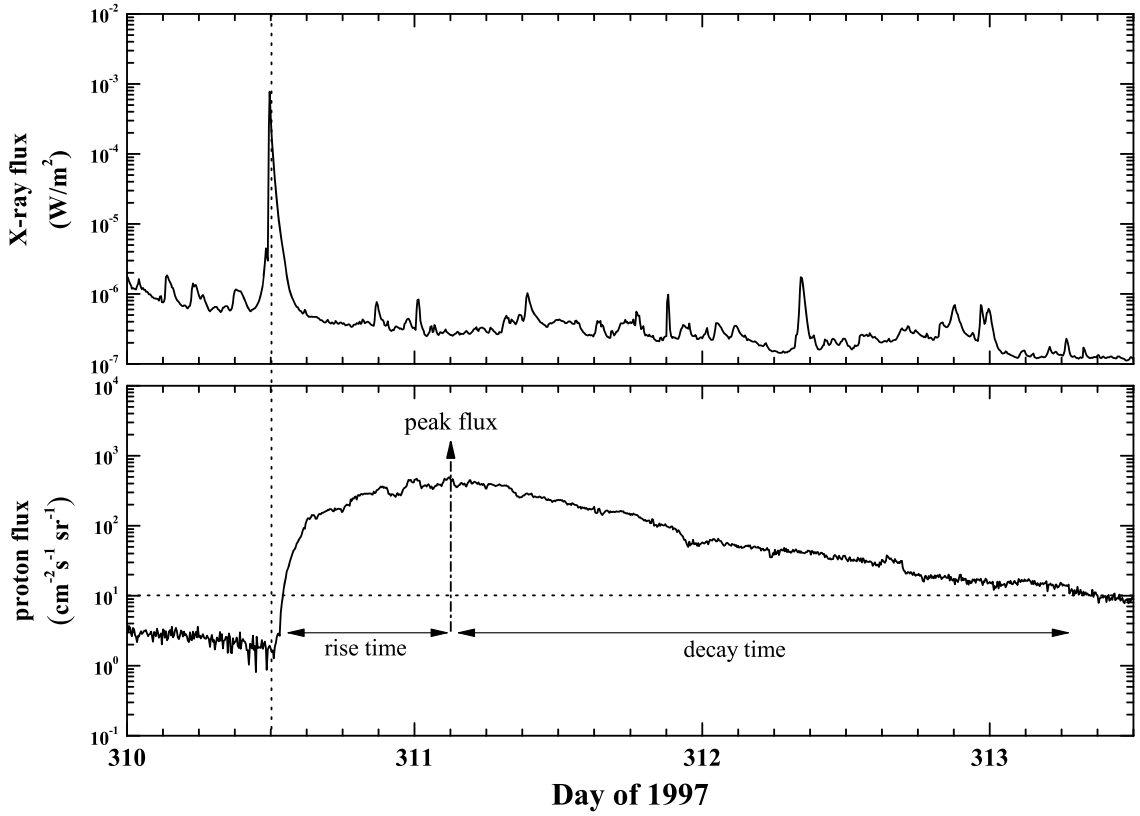

Figure 1. (top) GOES X-ray flux and (bottom panel) solar proton flux of a well-connected SPE on 6 November. The dot vertical line indicates the peak time of its associated X-ray flare. The dot horizontal line indicates the threshold (10 pfu) of SPE.

2.2. Model Description

For forecasting the solar proton flux profile, we compare several empirical functions such as probability density function and cumulative distribution function of Weibull distribution and Gaussian function. By comparing these functions with SPE profiles, we select a modified Weibull curve function. The formula for forecasting solar proton flux profile can be expressed as

$$F(t) = F_p \left(\frac{t}{\tau_r}\right) \exp\left[-\left(\frac{t}{\tau_r - \tau_d}\right)^2\right], \quad (1)$$

where F_p is the proton peak flux, τ_r is the rise time of proton flux profile, and τ_d is the decay time of proton flux profile.

We assume the start time of SPE flux profile (i.e., $t = 0$ at equation (1)) as 48 min after the peak time of its associated X-ray flare, which is an average of the differences between X-ray peak and SPE start times of 49 well-connected events.

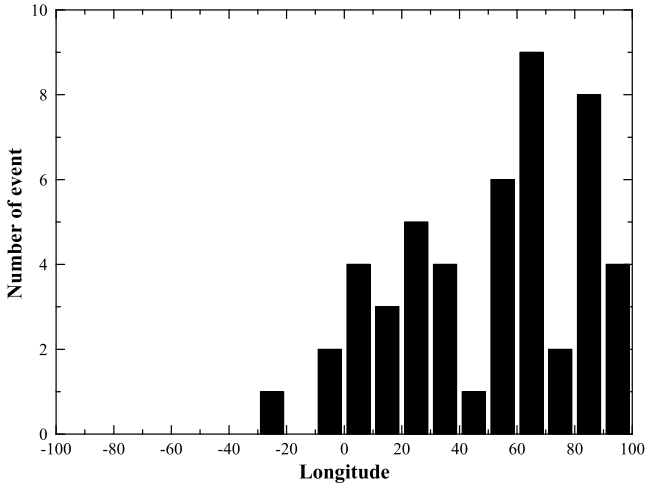

Figure 2. Histogram of longitudes of 49 well-connected SPEs.

2.2.1. Model Using Flare Parameters

To predict F_p in equation (1), we use the flare parameters such as X-ray flare peak flux, impulsive time, and emission measure (hereinafter referred to as Model 1). Here the impulsive time is a

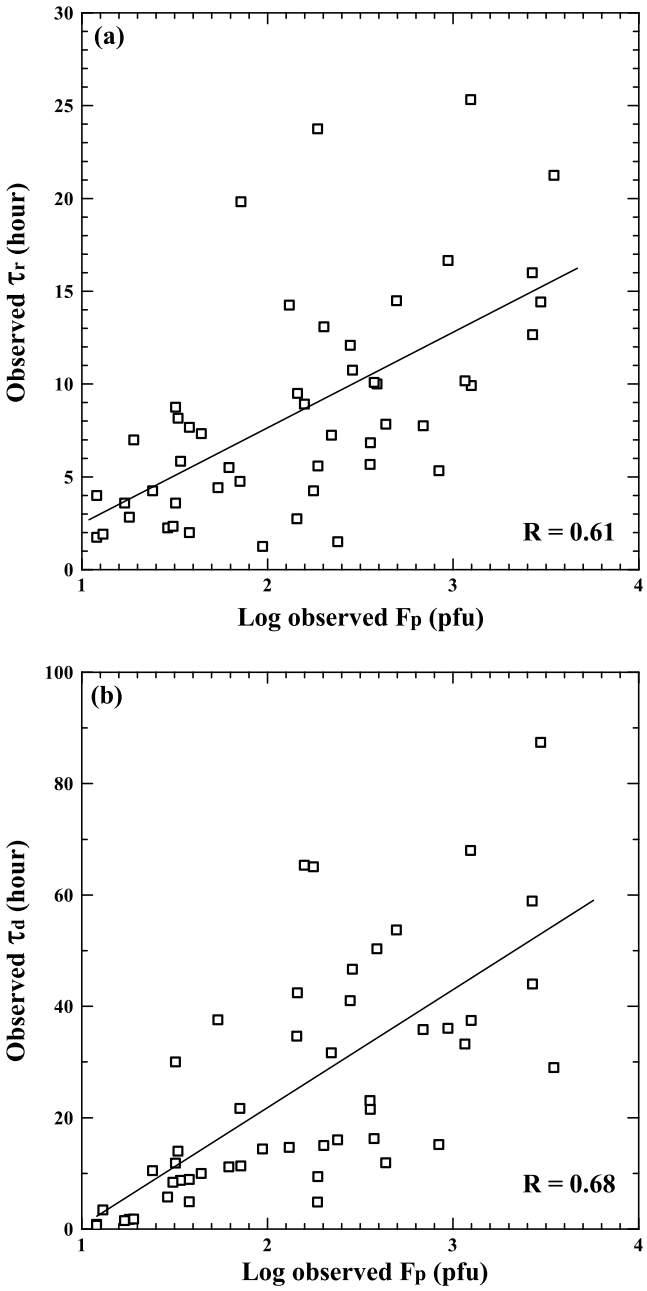

Figure 3. Relationship between two fitting parameters and proton peak flux of 49 well-connected SPEs: (a) observed τ_r and observed proton peak flux and (b) observed τ_d and observed proton peak flux.

proxy of flare duration that is defined as the time difference between flare start and peak time. The flare impulsive time is more useful than the flare duration in that it can be obtained at its peak time, which allow us to make a near-real-time proton event forecast [*Park et al.*, 2010]. From the multiple linear regression method using three flare parameters, F_p can be expressed as

$$\mathrm{Log}F_p = 0.84\,\mathrm{Log}F_x + 0.01T_i - 0.004\mathrm{EM} + 4.9, \quad (2)$$

where F_x is X-ray flare peak flux, T_i is the flare impulsive time (min), and EM is the flare emission measure ($\times 10^{49}$ cm^{-3}).

We predict the proton peak flux (F_p) using three flare parameters. We examine the relationship between observed two parameters (τ_r and τ_d) and observed proton peak fluxes of 49 well-connected SPEs in Figure 3. As seen in the figures, τ_r and τ_d have possible correlations with proton peak fluxes with $r = 0.61$ and $r = 0.68$. From these linear regressions, τ_r and τ_d can be expressed as

$$\tau_r = 62.02\,\mathrm{Log}F_p - 32.35 \quad (3)$$

$$\tau_d = 248.35\,\mathrm{Log}F_p - 237.8. \quad (4)$$

These equations show that if the proton peak flux is well predicted, then we can determine τ_r and τ_d from F_p. It is noted that the forecasts of F_p, τ_r, and τ_d can be made just after knowing F_x.

2.2.2. Model Using Flare and CME Parameters

We develop a second forecast model based on both flare and CME parameters (hereinafter referred to as Model 2). Besides three flare parameters, we use two CME parameters: CME linear speed and CME angular width. It is well known that the CME linear speed and its angular width are important factors for predicting SPEs [*Gopalswamy et al.*, 2003; *Cane et al.*, 2010; *Park et al.*, 2012]. We use 22 well-connected SPEs with CME information from 1997 to 2006. The CME linear speed and its angular width are taken from the SOHO/Large Angle and Spectrometric Coronagraph (LASCO) CME online catalogue (http://cdaw.gsfc.nasa.gov/CME_list/) [*Yashiro et al.*, 2004; *Gopalswamy et al.*, 2009].

To predict F_p, we use a multiple linear regression method using flare and CME parameters (X-ray flare peak flux, impulsive time, emission measure, source location, CME linear speed, and CME angular width). As a result, F_p can be expressed as

$$\mathrm{Log}F_p = 1.05\,\mathrm{Log}F_x + 0.01T_i - 0.01\mathrm{EM} - 0.008l + 0.2\times 10^{-3}V_{\mathrm{CME}} - 0.6\times 10^{-3}\mathrm{AW} + 6.2, \quad (5)$$

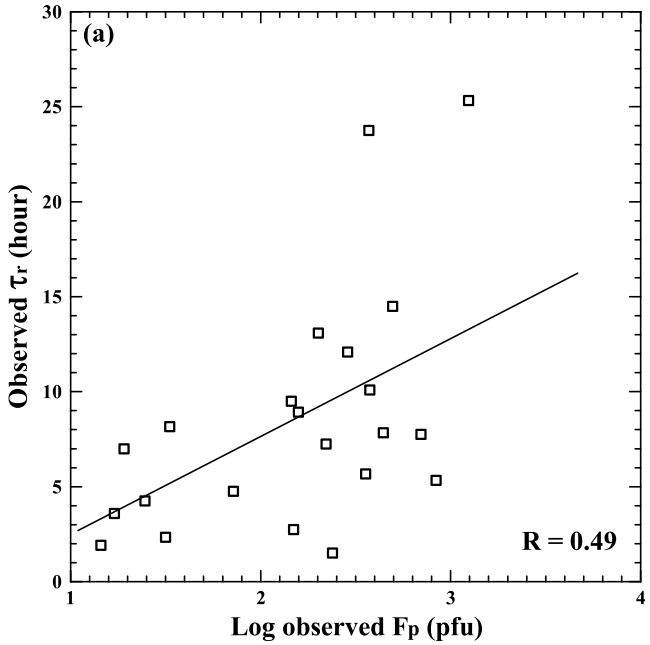

Figure 4. Relationship between two fitting parameters and proton peak flux of 22 well-connected SPEs: (a) observed τ_r and observed proton peak flux and (b) observed τ_d and observed proton peak flux.

where l is the longitude of its associated flare (west: + and east: −), V_{CME} is CME linear speed (km^{-1}), and AW is CME angular width (degree).

We examine the relationship between observed two parameters (τ_r and τ_d) and observed proton peak fluxes of 22 well-connected SPEs in Figure 4. As seen in the figures, τ_r and τ_d have possible correlations with proton peak fluxes with $r = 0.49$ and $r = 0.58$. Their correlations are not so high. From these linear regressions, τ_r and τ_d can be expressed as

$$\tau_r = 63.62\,\mathrm{Log}F_p - 35.01 \quad (6)$$

$$\tau_d = 234.74\,\mathrm{Log}F_p - 213.65, \quad (7)$$

3. Result and Discussion

Figure 5 shows a good example of predicted proton flux profile for Model 1. The source location of its associated X-ray flare is S07W62, and the X-ray peak flux is 5.5×10^{-5} W/m^2 (M5 class). The RMS (root-mean-square) errors between predicted and observed F_p, τ_r, and τ_d are 0.11 $\log_{10}$(pfu), 1.2 h, and 4.6 h, respectively. From these results, Model 1 successfully predicts the proton flux profile in the rise and decay phases as well as at its peak flux.

Figure 6 shows a bad example of predicted proton flux profile for Model 1. The source location of its associated X-ray flare is N09W17, and the X-ray peak flux is 2.09×10^{-4} W/m^2 (X2 class). As seen in Figure 6, the times of rise and decay phase predicted from the model are longer than the observed ones in the proton flux profile. Also, the predicted peak flux is smaller than the observed one. One interesting thing is that there is another enhancement of proton flux near 18:00 UT on 8 November, which may be related to a M2 class X-ray flare at 15:45 UT.

Figure 7 shows an example of predicted proton flux profile for Model 2. The source location of its associated X-ray flare is S18W63, and its peak flux is 7.7×10^{-4} W/m^2 (M9 class). The RMS errors between predicted and observed F_p, τ_r, and τ_d are 0.17 $\log_{10}$(pfu), 4.4 h, and 6.2 h, respectively. As seen in Figure 7, Model 2 approximately predicts the proton flux profile in the rise and decay phases as well as at its peak flux even if there are difference between the observed and predicted rise and decay phases.

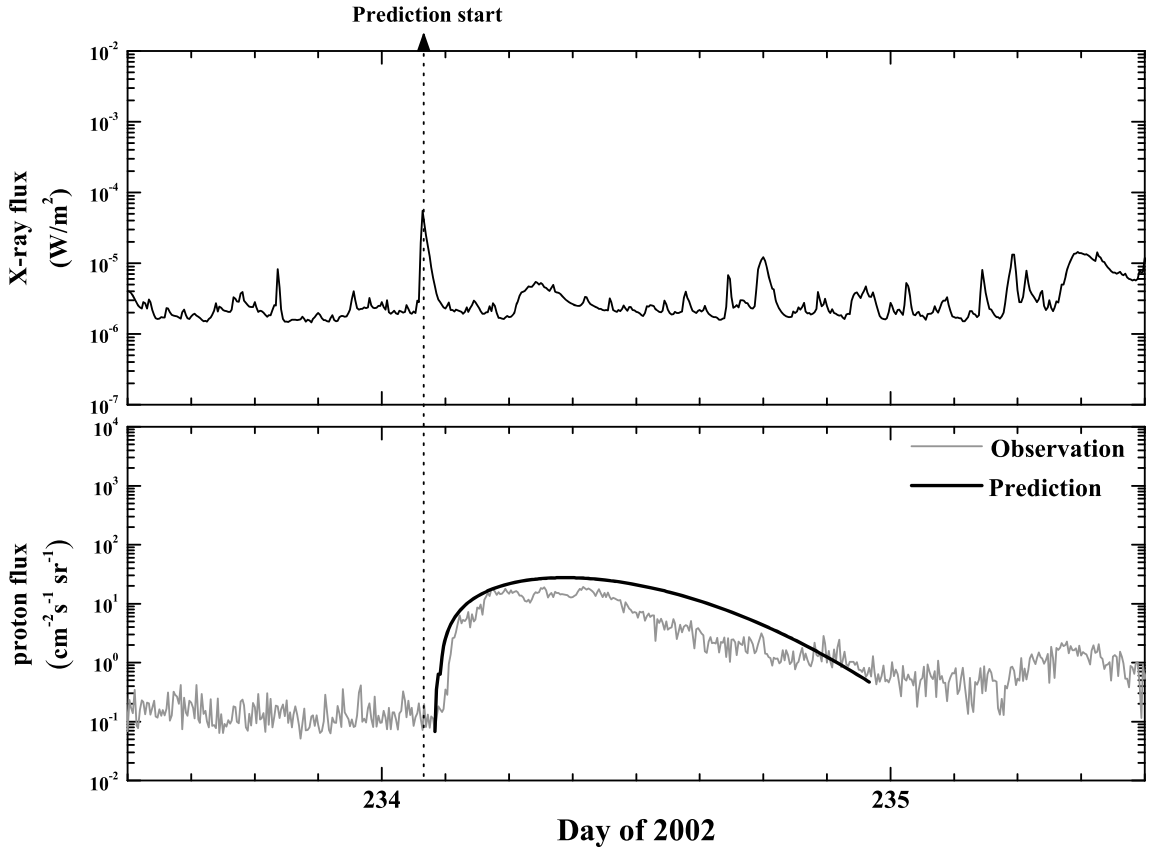

Figure 5. (top) GOES X-ray flux and (bottom) solar proton flux of a proton flux profile on 22 August 2002 for Model 1. The thick and thin solid lines indicate the predicted and observed proton flux data, respectively. The dotted vertical line indicates the peak time of its associated flare, which is the earliest time for the prediction of SPE profiles.

Figure 8 shows the relationship between predicted and observed proton peak fluxes with the correlation coefficient of 0.65 for Model 1. The RMS error and MAE (mean absolute error) between predicted and observed proton fluxes are 0.55 $\log_{10}$(pfu) and 0.45 $\log_{10}$(pfu), respectively. Figure 9 shows the relationship between predicted and observed proton peak fluxes for Model 2. As shown in the Figure 9, the predicted ones are very consistent with the observed with a good correlation coefficient of 0.83. The RMS error and MAE between predicted and observed proton fluxes are 0.35 $\log_{10}$(pfu) and 0.28 $\log_{10}$(pfu), respectively. From these results, we realize that Model 2 better predicts the proton peak fluxes than Model 1.

We compare the correlation coefficient between predicted and observed proton peak fluxes for our models with that of previous SPE forecast models: the proton prediction system (PPS) [*Kahler et al.*, 2007] and the SWPC proton prediction model [*Balch*, 2008]. The correlation coefficients between observed and predicted fluxes for PPS and SWPC proton prediction models are 0.55 [*Kahler et al.*, 2007] and 0.5 [*Balch*, 2008], respectively. The correlation coefficients (0.65 and 0.83) for our model are noticeably larger than those for the PPS and SWPC models. This result may come from why we consider only well-connected events.

Tables 1 and 2 show the RMS errors and uncertainty of regression between predicted and observed F_p, τ_r, and τ_d for Models 1 and 2. As for the RMS errors and uncertainty of regression of F_p for two models, we think that Models 1 and 2 can reasonably predict the proton peak flux. Comparing τ_r with τ_d, the RMS errors and uncertainty of regression of τ_r are much smaller than those of τ_d, which are relatively large in terms of the forecast of SPE profiles. We also find that the RMS errors and uncertainty of regression of F_p and τ_r for Model 2 are smaller than those of Model 1. The RMS errors and uncertainty of regression of τ_d for two models are similar to each other. In terms of the uncertainties of the models, the tables show that Model 2 has a better performance than Model 1.

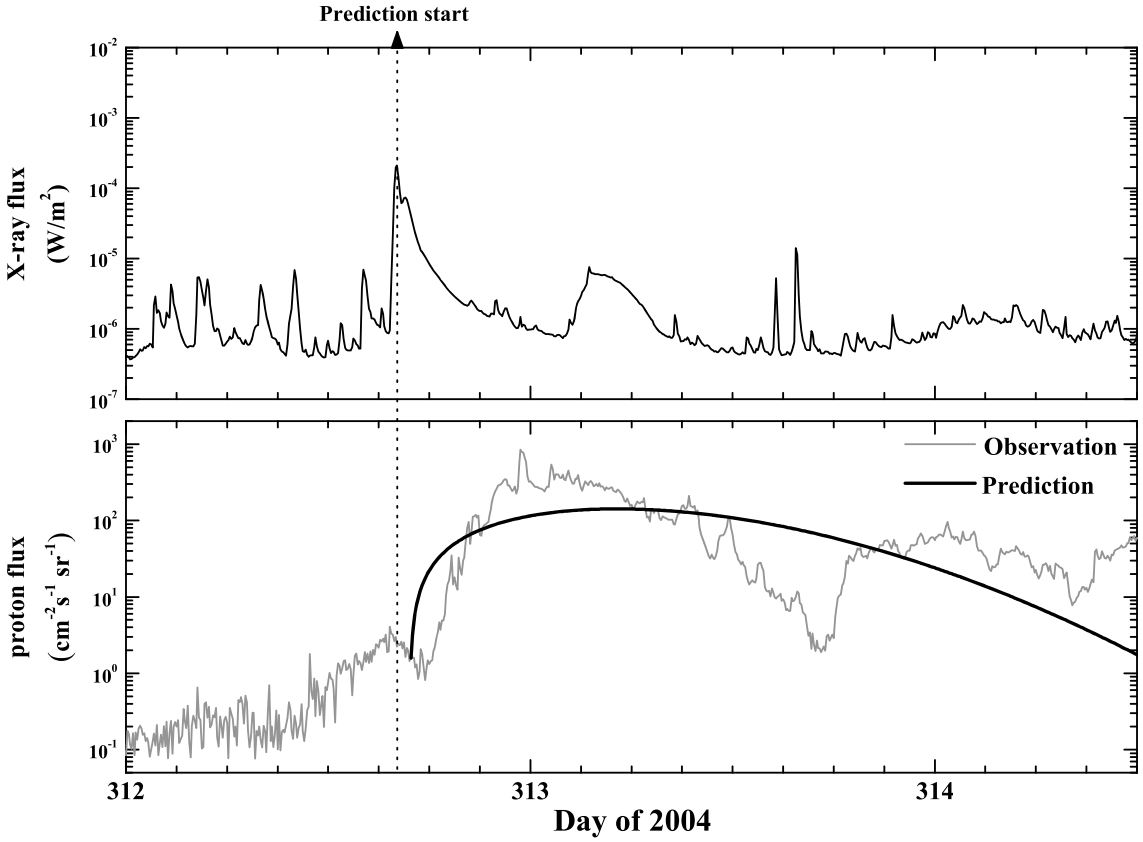

Figure 6. (top) GOES X-ray flux and (bottom) solar proton flux of a proton flux profile on 7 November 2004 for Model 1. The thick and thin solid lines indicate the predicted and observed proton flux data, respectively. The dotted vertical line indicates the peak time of its associated flare, which is the earliest time for the prediction of SPE profiles.

We examine the RMS errors between predicted and observed proton peak fluxes depending on longitude. We classify the well-connected SPEs into two groups: (1) 34 events (Group 1) are located between W30° and W90° and (2) 15 events (Group 2) are located at the other regions. We find that the RMS errors of Group 1 are 0.53 $\log_{10}$(pfu) and 0.29 $\log_{10}$(pfu) for two models, respectively. The RMS errors of Group 2 are 0.66 $\log_{10}$(pfu) and 0.49 $\log_{10}$(pfu) for two models, respectively. We see that the RMS errors for Group 1 are smaller than those of Group 2 for two models. We made a similar analysis for two groups: events whose time interval between X-ray peak and proton start times is less than 2 h and the others. It is also found that the first group of events have a smaller RMS error than the second group. An earlier onset at 1 AU can be explained by well-connected event and/or harder energy spectrum. If these two groups of events have similar distributions of energy spectrum, our results can be understood by the fact that the first group of events (or Group 1 events) are more well-connected events than the second group of events (or Group 2 events). Thus, we think that our models well predict the events occurring near sub-Earth point among well-connected SPEs.

We examine the relationship between observed duration ($\tau_r + \tau_d$) and observed proton peak fluxes ($\log F_p$) of 49 well-connected SPEs, and their correlation coefficient is 0.74. This fact implies a good correlation between proton peak flux and its duration. We also predict the proton flux profile using a linear equation obtained from the relationship between proton peak fluxes and its duration. We find that the results (correlation coefficient, RMS error, and MAE) for this case are equal to those from equations (3) and (4).

Table 3 shows the RMS errors between predicted and observed proton peak fluxes for Models 1 and 2. We see that the RMS errors of four events for Model 1 are larger than 1 in the $\log_{10}$ (Numbers 4, 13, 30, and 34 in Table 3). Although these events show typical characteristics of well-connected events, which have rapid increments in proton flux and originate from the western region, they have high RMS errors, which may be

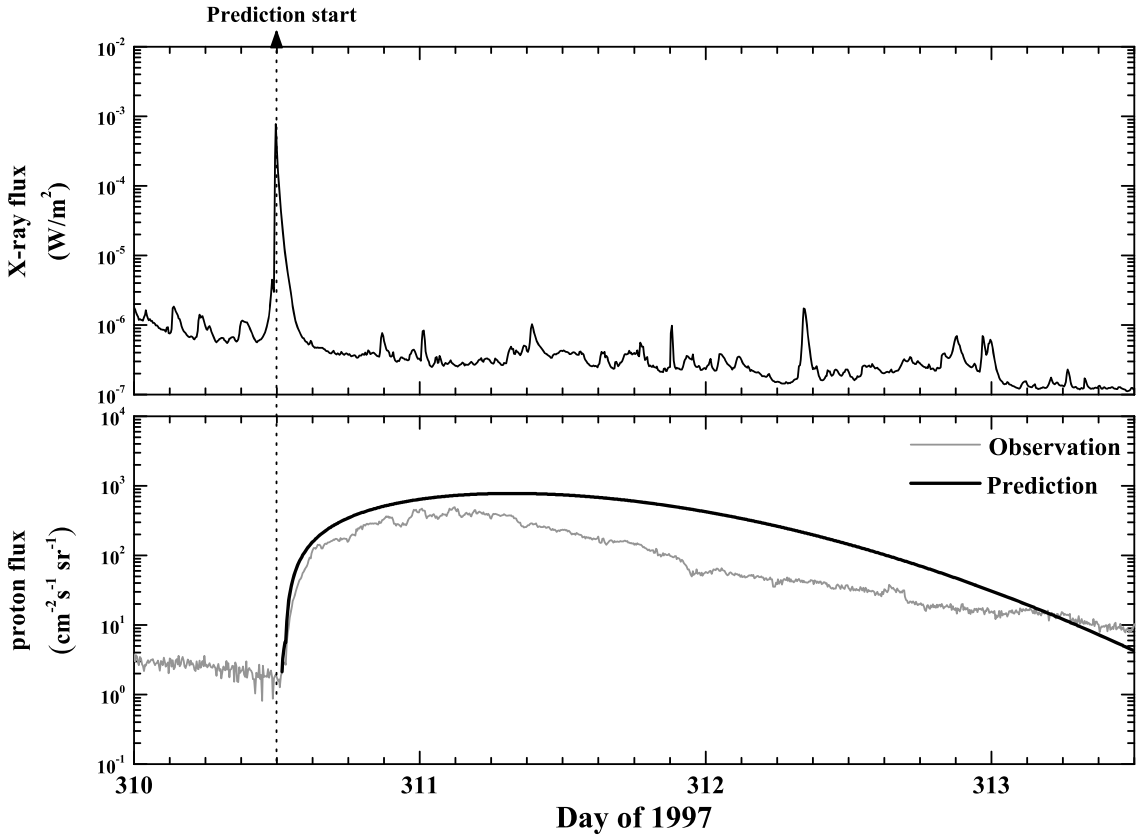

Figure 7. (top) GOES X-ray flux and (bottom) solar proton flux of a proton flux profile on 6 November 1997 for Model 2. The thick and thin solid lines indicate the predicted and observed proton flux data, respectively. The dotted vertical line indicates the peak time of its associated flare, which is the earliest time for the prediction of SPE profiles.

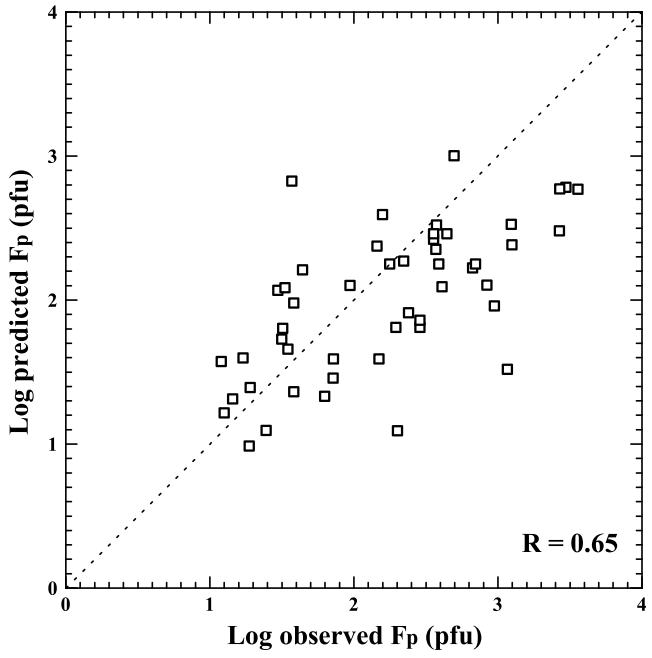

Figure 8. Relationship between predicted and observed proton peak fluxes for Model 1.

caused by additional flare and CME parameters. As one possibility, we examine the acceleration of the CME associated with Number 34 event, which is the only one having the CME information among four events. Its linear fit speed is 1550 km/s, and its second order speed at the final height is 1830 km/s. The estimated CME acceleration from second-order fit is 58.2 m/s^2, which is the largest among 13 SPEs except for the events (9/22) with uncertain estimates of accelerations. We examine the relationship between the error of Model 2 and CME acceleration using 13 events in Figure 10. As seen in Figure 10, the larger CME acceleration is, the larger $\triangle F_p$ is. From these results, we think that the CME acceleration parameter is also an important factor for predicting proton flux profile.

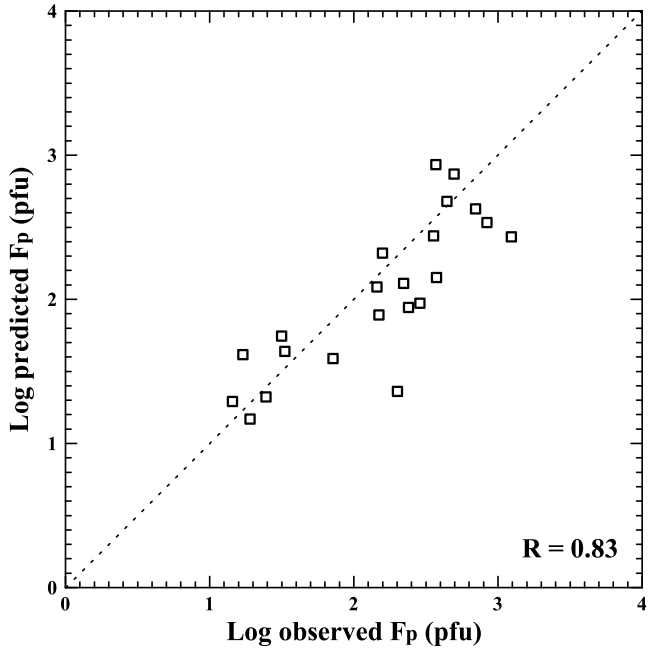

Figure 9. Relationship between predicted and observed proton peak fluxes for Model 2.

Based on the above results, we add the CME acceleration to Model 2 and predict proton flux profile using 22 SPEs. The formula can be expressed as

$$\begin{aligned}\mathrm{Log}F_p = {} & 1.2\,\mathrm{Log}F_x + 0.01T_i - 0.01\mathrm{EM} \\ & - 0.007I + 0.09\times 10^{-3}V_{\mathrm{CME}} \\ & - 0.1\times 10^{-3}\mathrm{AW} \\ & + 0.7\times 10^{-2}\mathrm{Accel} + 6.9,\end{aligned} \tag{8}$$

where Accel is CME acceleration (m s^{-2}).

For simplicity, we assume the accelerations of CMEs, which have uncertain estimates of CME acceleration, to be 0. In this case, the correlation coefficient between predicted and observed proton peak fluxes is 0.87. The RMS error is 0.33 $\log_{10}$(pfu), which is better than those for Models 1 and 2. From these results, we find that the CME acceleration is also a very important factor for predicting SPE profiles together with CME speed and width. It is noted that this case is only applicable when CME acceleration data are available.

Our models are similar to the UMASEP model developed by *Núñez* [2011] in that both models predicts proton flux profiles using empirical functions. For the estimation of uncertainty, we compute the RMS errors of peak fluxes of all events for our two models in Table 3. *Núñez* [2011] only reported the RMS error of flux at start time +7 h as a representative error of the UMASEP model in which he selected an empirical function with the best temporal length of 7 h. For comparison, we also estimate the RMS errors between predicted and observed proton flux at start time +7 h. The average of RMS errors for Model 1 is larger than that of UMASEP model (Model 1: 0.44 $\log_{10}$(pfu), UMASEP: 0.38 $\log_{10}$(pfu)). The average value of RMS errors for Model 2 is nearly similar to the value of UMASEP model (Model 2: 0.33 $\log_{10}$(pfu), UMASEP: 0.33 $\log_{10}$(pfu)). While the UMASEP model only predicts proton flux profiles during initial rise phases, our models can predict a SPE flux profile from rise to decay phase as well as SPE peak flux.

4. Summary and Conclusion

In this paper, we have developed two forecast models of solar proton flux profiles for well-connected events. For this study, we have selected 49 well-connected events among SPEs from 1986 to 2006. In particular, we have compared the predicted and observed peak fluxes using correlation coefficient (CC), RMS error, MAE, and uncertainty of regression. The main results from this study can be summarized as follows.

Our models successfully predict the proton flux profiles of well-connected SPEs in terms of their peaks, rise, and decay times. The CC, RMS error, MAE, and uncertainty of regression between the predicted and observed proton peak fluxes for Model 1 are 0.65, 0.55 $\log_{10}$(pfu), 0.45 $\log_{10}$(pfu), and 0.58 $\log_{10}$(pfu), respectively. The CC, RMS error, MAE, and uncertainty of regression for Model 2 are 0.83, 0.35 $\log_{10}$(pfu), 0.28 $\log_{10}$(pfu), and 0.37 $\log_{10}$(pfu), respectively. These results show that Model 2 is noticeably

Table 1. RMS Errors and Uncertainty of Regression of F_p, τ_r, and τ_d for Model 1

	RMS Error	Uncertainty of Regression
F_p	0.55 $\log_{10}$(pfu)	0.58 $\log_{10}$(pfu)
τ_r	6.5 h	6.7 h
τ_d	17.2 h	17.6 h

Table 2. RMS Errors and Uncertainty of Regression of F_p, τ_r, and τ_d for Model 2

	RMS Error	Uncertainty of Regression
F_p	0.35 $\log_{10}$(pfu)	0.37 $\log_{10}$(pfu)
τ_r	6.0 h	6.3 h
τ_d	17.4 h	18.2 h

better than Model 1, which are consistent with previous results on the intimate relationship between CME parameters and SPE occurrence [*Park et al.*, 2012].

Even though the RMS error and uncertainty of regression for Model 1 are higher than those of Model 2, Model 1 is

Table 3. Input Data and RMS Errors of Models 1 and 2

Number	SPE Start Time (UT)	Flare Peak Time (UT)	CME Speed (km/s)	RMS Error ($\log_{10}$(pfu)) Model 1	Model 2
1	19860206 0845	19860206 0625		0.48	
2	19860214 1025	19860214 0935		0.64	
3	19860504 1220	19860504 1005		0.28	
4	19880102 2245	19880102 2145		1.25	
5	19880630 0950	19880630 0905		0.11	
6	19890317 1855	19890317 1740		0.71	
7	19890323 2005	19890323 1955		0.59	
8	19890725 0845	19890725 0840		0.29	
9	19890929 1145	19890929 1130		0.68	
10	19891019 1305	19891019 1255		0.94	
11	19891115 0705	19891115 0700		0.39	
12	19891130 1335	19891130 1230		0.78	
13	19900319 0610	19890319 0455		1.01	
14	19900521 2245	19900521 2215		0.51	
15	19900524 2100	19900524 2050		0.001	
16	19910225 0905	19910225 0815		0.49	
17	19910513 0215	19910513 0140		0.13	
18	19911030 0655	19911030 0630		0.12	
19	19920625 2015	19920625 2010		0.33	
20	19921030 1830	19921030 1815		0.65	
21	19930312 1835	19930312 1810		0.56	
22	19940220 0150	19940220 0140		0.26	
23	19941020 2150	19941019 2125		0.11	
24	19951020 0640	19951020 0605		0.46	
25	19971104 0645	19971104 0555	785	0.39	0.26
26	19971106 1225	19971106 1155	1556	0.3	0.17
27	19980502 1350	19980502 1340	938	0.58	0.28
28	19980506 0815	19980506 0810	1099	0.46	0.43
29	19980824 2300	19980824 2210		0.59	
30	19980930 1415	19980930 1345		1.54	
31	19990604 0835	19990604 0700	2230	0.29	0.06
32	20000610 1720	20000610 1700	1108	0.22	0.24
33	20000722 1215	20000722 1130	1230	0.15	0.13
34	20000912 1355	20000912 1210	1550	1.21	0.94
35	20010128 1710	20010128 1600	916	0.56	0.11
36	20010402 2250	20010402 2150	2505	0.39	0.12
37	20010410 0745	20010410 0525	2411	0.21	0.36
38	20010415 1350	20010415 1350	1199	0.05	0.42
39	20011226 0545	20011226 0545	1446	0.09	0.11
40	20020421 0145	20020421 0145	2393	0.56	0.66
41	20020822 0230	20020822 0155	998	0.11	0.11
42	20020824 0120	20020824 0110	1913	0.07	0.23
43	20030531 0225	20030531 0225	1835	0.36	0.38
44	20031026 1825	20031026 1810	1537	0.18	0.03
45	20031104 2225	20031104 1945	2657	0.21	0.07
46	20041107 1805	20041107 1605	1759	0.81	0.39
47	20050616 2025	20050616 2020		0.21	
48	20050822 1905	20050822 1725	2378	0.59	0.48
48	20061213 0250	20061213 0240	1774	0.59	0.21

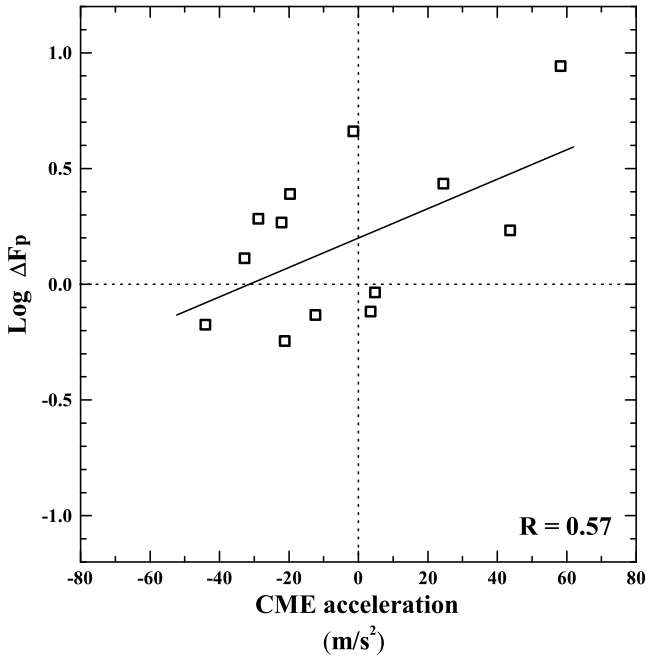

Figure 10. Relationship between the CME acceleration and $\triangle F_p$ for Model 2. $\triangle F_p$ is the difference between the observed and predicted proton peak fluxes ($\triangle F_p$ = log F_p(observed) − log F_p(predicted)).

still important for space weather forecast since it is possible to forecast SPE flux profiles just after the peak times of their associated flares using GOES X-ray flux data. In case of Model 2, CME parameters can be determined with the help of a software such as CME analysis tool of NOAA SWPC using SOHO/LASCO and/or STEREO/SECCHI, which are available at about 12–20 min after the CME observations. As for the forecast of SPE flux profiles, it is very important to make a near-real-time analysis of CME parameters. Therefore, it would be recommendable to make a two-stage forecast: Model 1 just after the X-ray peak time and Model 2 after the availability of CME speed and angular width.

Our models predict the SPE flux profiles when their associated X-ray (> M1) flares occur. In fact, many flares stronger than M1 class are not always associated with SPEs. Thus, we suggest using our models together with SPE probability models [e.g., *Park et al.*, 2010, 2012] for space weather operations. We expect that while the SPE probability models provide its occurrence probability depending on flare and CME parameters, our models can forecast the proton flux profiles when SPE occurrence probability is high enough to occur.

Acknowledgments

This work was supported by the BK21 plus program through the National Research Foundation (NRF) funded by the Ministry of Education of Korea, Basic Science Research Program through the NRF funded by the Ministry of Education (NRF-2013R1A1A2012763), NRF of Korea grant funded by the Korean Government (NRF-2013M1A3A3A02042232), Research grant funded by Korea Polar Research Institute (PE15010). The data used in this study are available at NOAA NGDC (ftp://ftp.ngdc.noaa.gov/STP/space-weather/solar-data/solar-features/solar-flares/x-rays/goes/) for GOES data, NOAA SWPC (http://www.swpc.noaa.gov/ftpdir/indices/SPE.txt) for SPEs, and SOHO LASCO CME online catalogue (http://cdaw.gsfc.nasa.gov/CME list/) for CMEs.

Yuming Wang thanks Linghua Wang and another reviewer for their assistance in evaluating this paper.

References

Aran, A., B. Sanahuja, and D. Lario (2005), A first step towards proton flux forecasting, *Adv. Space Res.*, *36*, 2333–2338.

Balch, C. C. (1999), SEC proton prediction model: Verification and analysis, *Radiat. Meas.*, *30*, 231–250.

Balch, C. C. (2008), Updated verification of the Space Weather Prediction Ceter's solar energetic particle prediction model, *Space Weather*, *6*, S01001, doi:10.1029/2007SW000337.

Beeck, J., G. M. Mason, D. C. Hamilton, G. Wibberenz, H. Kunow, D. Hovestadt, and B. Klecker (1987), A multispacecraft study of the injection and transport of solar energetic particles, *Astrophys. J.*, *322*, 1052–1072.

Cane, H. V., and D. Lario (2006), An introduction to CMEs and energetic particles, *Space Sci. Rev.*, *123*, 45–56.

Cane, H. V., I. G. Richardson, and T. T. von Rosenvinge (2010), A study of solar energetic particle events of 1997-2006: Their composition and associations, *J. Geophys. Res.*, *115*, A08101, doi:10.1029/2009JA014848.

Ding, L., Y. Jiang, L. Zhao, and G. Li (2013), The "Twin-CME" scenario and large solar energetic particle events in solar cycle 23, *Astrophys. J.*, *763*(1), 30.

Ding, L., G. Li, L. Dong, Y. Jiang, Y. Jian, and B. Gu (2014), On the identification of time interval threshold in the twin-CME scenario, *J. Geophys. Res. Space Physics*, *119*, 1463–1475, doi:10.1002/2013JA019745.

Feynman, J., and S. B. Gabriel (2000), On space weather consequences and predictions, *J. Geophys. Res.*, *105*, 10,543–10,564.

Garcia, H. A. (2004a), Forecasting methods for occurrence and magnitude of proton storms with solar soft X rays, *Space Weather*, *2*, S02002, doi:10.1029/2003SW000001.

Garcia, H. A. (2004b), Forecasting methods for occurrence and magnitude of proton storms with solar hard X rays, *Space Weather*, *2*, S06003, doi:10.1029/2003SW000035.

Gopalswamy, N., S. Yashiro, A. Lara, M. L. Kaiser, B. J. Thompson, P. T. Gallagher, and R. A. Howard (2003), Large solar energetic particle events of cycle 23: A global view, *Geophys. Res. Lett.*, *30*(12), 8015, doi:10.1029/2002GL016435.

Gopalswamy, N., S. Yashiro, G. Michalek, G. Stenborg, A. Vourlidas, S. Freeland, and R. Howard (2009), The SOHO/LASCO CME catalog, *Earth Moon Planet*, *104*, 295–313.

Heras, A. M., B. Sanahuja, Z. K. Smith, T. Detman, and M. Dryer (1992), The influence of the large-scale interplanetary shock structure on a low-energy particle event, *Astrophys. J.*, *391*, 359–369.

Kahler, S. W., E. W. Cliver, and A. G. Ling (2007), Validating the proton prediction system (PPS), *J. Atmos. Sol. Terr. Phys.*, *69*, 43–49.

Kahler, S. W., and A. Vourlidas (2013), A comparison of the intensities and energies of gradual solar energetic particle events with the dynamical properties of associated coronal mass ejections, *Astrophys. J.*, *769*(2), 143.

Kahler, S. W., and A. Vourlidas (2014), Solar energetic particle events in different types of solar wind, *Astrophys. J.*, *791*, 4.

Lario, D., B. Sanahuja, and A. M. Heras (1998), Energetic particle events: Efficiency of interplanetary shocks as 50 keV < E < 100 MeV proton accelerators, *Astrophys. J.*, *509*, 415–434.

Laurenza, M., E. W. Cliver, J. Hewitt, M. Storini, A. G. Ling, C. C. Balch, and M. L. Kaiser (2009), A technique for short-term warning of solar energetic particle events based on flare location, flare size, and evidence of particle escape, *Space Weather*, *7*, S04008, doi:10.1029/2007SW000379.

Luhmann, J. G., S. A. Ledvina, D. Krauss-Varban, D. Odstrcil, and P. Riley (2007), A heliospheric simulation-based approach to SEP source and transport modeling, *Adv. Space Res.*, *40*, 295–303.

Luhmann, J. G., S. A. Ledvina, D. Odstrcil, M. J. Owens, X.-P. Zhao, Y. Liu, and P. Riley (2010), Cone model-based SEP event calculations for application to multipoint observations, *Adv. Space Res.*, *46*, 1–21.

Núñez, M. (2011), Predicting solar energetic proton events (E > 10 MeV), *Space Weather*, *9*, S07003, doi:10.1029/2010SW000640.

Park, J., Y.-J. Moon, D.-H. Lee, and S. Youn (2010), Dependence of solar proton events on their associated activities: Flare parameters, *J. Geophys. Res.*, *115*, A10105, doi:10.1029/2011JA015330.

Park, J., Y.-J. Moon, and N. Gopalswamy (2012), Dependence of solar proton events on their associated activities: Coronal mass ejection parameters, *J. Geophys. Res.*, *117*, A08108, doi:10.1029/2011JA017477.

Reames, D. V. (1999), Particle acceleration at the Sun and in the heliosphere, *Space Sci. Rev.*, *90*, 413–491.

Reames, D. V. (2013), The two sources of solar energetic particles, *Space Sci. Rev.*, *175*, 53–92.

Smart, D. F., and M. A. Shea (1989), PPS-87-A new event oriented solar proton prediction model, *Adv. Space Res.*, *9*, 281–284.

Verkhoglyadova, O. P., G. Li, G. P. Zank, Q. Hu, and R. A. Mewaldt (2009), Using the PATH code for modeling grandual SEP events in the inner heliosphere, *Astrophys. J.*, *693*, 894–900.

Verkhoglyadova, O. P., G. Li, G. P. Zank, Q. Hu, C. M. S. Cohen, R. A. Mewaldt, G. M. Mason, D. K. Haggerty, T. T. von Rosenvinge, and M. D. Looper (2010), Understanding large SEP events with the PATH code: Modeling of the 13 December 2006 SEP event, *J. Geophys. Res.*, *115*, A12103, doi:10.1029/2010JA015615.

Xapsos, M. A., G. P. Summers, and E. A. Burke (1998), Probability model for peak fluxes of solar proton events, *IEEE Trans. Nucl. Sci.*, *45*, 2948–2953.

Yashiro, S., N. Gopalswamy, G. Michalek, O. C. St. Cyr, S. P. Plunkett, N. B. Rich, and R. A. Howard (2004), A catalog of white light coronal mass ejections observed by the SOHO spacecraft, *J. Geophys. Res.*, *109*, A07105, doi:10.1029/2003JA010282.